Prepared for submission to JCAP
Accepted by JCAP

arXiv:1407.1137v1 [astro-ph.CO] 4 Jul 2014

Statistics of Dark Matter Halos in the Excursion Set Peak Framework

A. Lapi[a,b] **L. Danese**[b]

[a]Dip. Fisica, Univ. 'Tor Vergata', Via Ricerca Scientifica 1, 00133 Roma, Italy
[b]SISSA, Via Bonomea 265, 34136 Trieste, Italy

E-mail: lapi@sissa.it, danese@sissa.it

Abstract. We derive approximated, yet very accurate analytical expressions for the abundance and clustering properties of dark matter halos in the excursion set peak framework; the latter relies on the standard excursion set approach, but also includes the effects of a realistic filtering of the density field, a mass-dependent threshold for collapse, and the prescription from peak theory that halos tend to form around density maxima. We find that our approximations work excellently for diverse power spectra, collapse thresholds and density filters. Moreover, when adopting a cold dark matter power spectra, a tophat filtering and a mass-dependent collapse threshold (supplemented with conceivable scatter), our approximated halo mass function and halo bias represent very well the outcomes of cosmological $N-$body simulations.

Keywords: dark matter theory — galaxy formation — galaxy clustering

Contents

1 Introduction **1**

2 The excursion set peak framework **2**
2.1 Upcrossing in place of first crossing 4
2.2 Peaks as special positions 6

3 Approximated excursion set peak **6**
3.1 Halo bias 9

4 Summary **10**

A Excursion set peak parameters **10**
A.1 Scale-invariant power spectrum 11
A.2 Cold DM power spectrum 12

1 Introduction

According to the standard paradigm, galaxies and galaxy systems form when baryons settle within the gravitational potential wells constituted by virialized dark matter (DM) 'halos'. To deeply understand the abundance and clustering properties of these halos is a fundamental step toward formulating a sensible theory for the formation and evolution of cosmic structures in the Universe.

The issue is very complex, and its attack ultimately requires brute-force $N-$body simulations (see [1–7]); however, some analytic grasp is essential to physically interpret their outcomes, to provide approximated yet flexible analytic representations of the results, to develop strategies for future setups, and to quickly explore the effect of modifying the background cosmological/cosmogonical model.

In this vein, two main frameworks have been developed: the excursion set approach (see [8–16]), and peaks theory (see [17–20]). Basically, the former statistically describes the mass fraction in the density field which is above a critical threshold for collapse when conveniently smoothed on a certain scale. The latter envisages that halos form around special positions in space, and specifically around the peaks of the density field. Actually, the prescriptions from the two approaches can be merged in a unified framework, constituting a sort of excursion set theory for peaks, or excursion set peaks in brief (see [14, 17, 21, 22]). Recently, it has been shown that, with reasonable assumptions on the collapse history of halos, such a framework can be extremely effective in reproducing the outcomes of cosmological $N-$body simulations (see [23]).

Unfortunately, the results of the excursion set peak framework cannot be put in closed analytic form; this would be particularly useful to inspire consistent fitting formulae of the simulation outcomes, to provide flexible descriptions for different background cosmologies, and to easily derive other statistical quantities of interest, like halo merger rates. The main goal of this paper is to present approximated, yet very accurate analytical expressions for the halo abundance and bias in the excursion set peak framework.

Our working plan is straightforward: in section 2 we recall the basics of the excursion set approach, of peaks theory, and of their connection in the excursion set peak framework; in section 3 we present our analytic approximation to the excursion set peak, compare it to the exact results and to the outcomes of cosmological $N-$body simulations; in section 4 we summarize our findings.

As to cosmology we adopt the standard, flat Universe (see [24]) with matter density parameter $\Omega_M = 0.32$, baryon density parameter $\Omega_b = 0.05$, and Hubble constant $H_0 = 100\,h$ km s^{-1} Mpc^{-1} with $h = 0.67$. As to cosmogony, we adopt the standard cold DM power spectrum $P(k)$ by [18] with the correction for baryons by [25], normalized in such a way that the r.m.s. $\sigma(R) \equiv \sqrt{S(R)}$ takes on the value $\sigma_8 = 0.82$ on a scale $R = 8\,h^{-1}$ Mpc.

2 The excursion set peak framework

In this Section we recall the basics of the excursion set peak framework, highlight some delicate points useful in the sequel, and set the notation. The expert reader may jump directly to section 3.

We consider a Gaussian initial field of fluctuations with overdensity $\delta \equiv \rho/\bar{\rho} - 1$ relative to the background $\bar{\rho}$; we indicate with δ_R the overdensity field smoothed on some scale R through a filter function $W_R(r)$ enclosing a volume $V = 4\pi \int \mathrm{d}r\, r^2\, W_R(r) \propto R^3$. The variance of this field

$$S_R \equiv \langle \delta_R^2 \rangle = \int \frac{\mathrm{d}k}{2\pi^2}\, k^2\, P(k)\, W_R^2(k)\ , \tag{2.1}$$

is determined by the Fourier transform of the filter $W_R(k)$ and by the power spectrum $P(k)$; for the spectra of interest in cosmology, S_R is an inverse, monotonic function of R.

The excursion set approach bases on the notion that, as the smoothing scale R decreases from large values, δ_R executes a random walk as a function of the increasing variable S_R (e.g., [8, 11, 12]); an example is illustrated in figure 1. The theory envisages that a halo with mass $M = \bar{\rho}\, V$ is formed when the walk first crosses a barrier $B(S,t)$ with general shape

$$B(S,t) = \delta_c(t)\, \left[1 + \beta\, \left(\frac{S}{\delta_c^2}\right)^{\eta}\right] = \nu\, (1 + \beta\, \nu^{-2\eta})\ . \tag{2.2}$$

Here $\delta_c(t)$ is the critical threshold for collapse extrapolated from linear perturbation theory; at the current epoch $\delta_c \approx 1.686$ holds, although the precise value weakly depends on cosmological parameters, and then it evolves like $\delta_c(t) \propto 1/D(t)$ with the cosmological time t, in terms of the linear growth function $D(t)$, see [26] for details.

The dependence of the barrier on the scale S is specified by the parameters (β, η), that are commonly set basing on the classic theory of halo collapse and/or on comparison with numerical simulation. The value $\beta = 0$ corresponds to a constant barrier that describes the standard spherical collapse ([8, 15]). On the other hand, numerical simulations indicate the collapse is rather ellipsoidal (if not triaxial); correspondingly, the barrier features a nonlinear shape with typical values $\beta \approx 0.5$ and $\eta \approx 0.45 - 0.65$. Note that the constraints on the slope η are rather loose, and the value $\eta = 0.5$ marking a 'square-root barrier' is often adopted because of its simplicity (cf. section 2.1), and to avoid delicate normalization issues (for $\eta > 1/2$ not all walks are guaranteed to cross the barrier since the r.m.s. height scales like $\sqrt{S}$). Actually, simulations also show that the barrier $B(S,t)$ at given S features some scatter, whose ultimate nature is currently unknown (see [1, 27, 28]). The last equality in

eq. (2.2) highlights that these barriers can be recast in self-similar terms with the use of the variable $\nu \equiv \delta_c(t)/\sqrt{S}$; this is useful to treat simultaneously different epochs and/or masses[1].

According to the excursion set prescription, the halo mass function, i.e. the number density of halos of given mass M, is given by

$$\frac{\mathrm{d}N}{\mathrm{d}M} = \frac{\bar{\rho}}{M^2} \left| \frac{\mathrm{dlog}\nu}{\mathrm{dlog}M} \right| \nu\, f(\nu) \; ; \tag{2.3}$$

here $f(S) = f(\nu)\,|\mathrm{d}\nu/\mathrm{d}S| = \nu\, f(\nu)/2\, S$ is the first crossing distribution, i.e., $f(S)\,\mathrm{d}S$ represents the probability that a trajectory crosses the barrier for the first time between S and $S + \mathrm{d}S$. Since there is a one-to-one correspondence between the halo mass function and the first crossing distribution, in the rest of the paper we will present our results in terms of the latter.

As to the filter function, the simplest choice is a tophat filter in Fourier space $W_R(k) \propto \theta_{\rm H}(k_R - k)$, with $\theta_{\rm H}(\cdot)$ the Heaviside step function and $k_R \propto 1/R$ a cutoff wavenumber; the resulting random walk is purely Markovian, with no correlation between the steps. Such a 'sharp $k-$space filter' have been adopted at large in the past literature since it allows to derive analytically exact expressions of the mass function for simple barrier shapes (e.g., constant, square-root or linear). For other nonlinear barriers the result is only numerical (e.g., [29–31]) but can be approximated analytically (see [11]) in the mass range relevant for cosmological studies. However, the outcome with this filter is somewhat unsatisfactory, mainly for two reasons: (i) the filter is unrealistic since the enclosed volume V (hence the mass M) is ill-defined or, at least, ambiguous; (ii) a general agreement with the mass function from cosmological simulations can be obtained only after rescaling the nonlinear barrier of eq. (2.2) by an ad-hoc factor $\sqrt{q}$ with $q \approx 0.7$.

Admittedly, a tophat filter in real space $W_R(r) \propto \theta_{\rm H}(R-r)$ offers a more direct contact with the standard theory of nonlinear halo collapse, and a fairer comparison with numerical simulations since better reflects the way halos are identified into them[2]. The corresponding Fourier transform of the tophat filter which enters eq. (2.1) reads

$$W_R(k) = 3\, \frac{\sin kR - kR\cos kR}{(kR)^3} \; ; \tag{2.4}$$

this filter encloses a finite and well-defined volume $V = 4\pi\, R^3/3$, although for some power spectra it can produce a smoothed density field which is not locally differentiable with respect to r. To circumvent the issue, it is standard to multiply the above expression by a small-scale Gaussian $e^{-\epsilon\, k^2/2}$ with $\epsilon \lesssim 0.1$, that smooths the sharp edges of the tophat (see [8, 12, 13]). Another filtering, which is commonly used in peaks theory, is constituted by a pure Gaussian function $W_R(k) = e^{k^2\, R^2/2}$, which plainly produces a differentiable smoothed density field and encloses a volume $V = (2\pi)^{3/2}\, R^3$.

[1] Note that in the literature on the excursion set approach, including our paper [11], the variable ν is often defined as δ_c^2/S; here instead we adopt the standard notation of the excursion set peak framework and define $\nu \equiv \delta_c/\sqrt{S}$.

[2] As shown by [5] and many other authors, the first crossing distribution extracted from $N-$body simulations depends on the way halos are identified; in this work we always refer to the $N-$body outcome for halos identified via a spherical overdensity algorithm with a nonlinear contrast $\Delta \approx 200$. This can be fairly compared with the excursion set results for a real-space top-hat filtering and a linear density contrast $\delta_c \approx 1.686$.

With the tophat and gaussian filter, the random walk executed by δ_R as a function of S_R is no longer Markovian, and correlations between the steps are introduced. The quantity

$$C_{R,R'} \equiv \langle \delta_R \delta_{R'} \rangle = \int \frac{\mathrm{d}k}{2\pi^2}\, k^2\, P(k)\, W_R(k)\, W_{R'}(k)\ , \tag{2.5}$$

gauges the strength of these correlations; the outcome is that random walks with correlations tends to vary less erratically than the Markovian one, as can be seen in the examples illustrated in figure 1.

Moreover, the numerical and analytic techniques to derive the first crossing distribution in the Markovian case cannot be applied when correlations between the steps are present, and other kinds of computations must be employed.

2.1 Upcrossing in place of first crossing

A Montecarlo approach is the most direct way to derive the first crossing distribution (see [8, 32]); this exploits the fact that the probability of a trajectory to reach a location $(\delta_{R+\Delta R}, S_{R+\Delta R})$ starting from (δ_R, S_R) is simply given by a gaussian with mean $C_{R,R+\Delta R}\,\delta_R/S_R$ and variance $[S_{R+\Delta R} - C^2_{R,R+\Delta R}/S_R]^{1/2}$. The Montecarlo algorithms runs as follows: a set (typically 10^5 realizations are enough) of walks is constructed by extracting randomly the increment in δ_R at each step in S_R from the above distribution; then each walk is evolved until it first crosses the barrier at a given location S; the number of walks crossing the barrier between S and $S + \Delta S$, divided by ΔS and by the number of overall realization, is the first crossing distribution $f(S)$. Such a Montecarlo scheme has the advantage of providing the *exact* (i.e., not approximated) first crossing distribution, although the outcome is only numerical, and the required computational time may become long when massive use of $f(S)$ is needed.

To circumvent the issue, some analytic approximations have been developed in the literature, aimed at reproducing the outcomes of the Montecarlo computation above. A simple and rather accurate one has been originally proposed by [8] for a constant barrier, and then extended to nonlinear barriers by [13]. The idea is to approximate the 'first crossing' distribution $f(S)$ with the 'upcrossing' one, i.e., the distribution of walks crossing the barrier from below, irrespective of earlier crossings. The bottom line is that when correlations between the steps are present, the random walk does not exhibit the frenetic variations of the Markovian case; thus if it crosses the barrier from below at S, it is very likely that no crossing has occurred for $S' < S$, and especially so at small S.

Quantitatively, one has to compute the fraction of walks with the requirements that $\delta_R > B(S_R)$ and $\delta_{R+\Delta R} < B(S_{R+\Delta R})$ for small ΔR. This translates into $f(S) \simeq \int_{\dot{B}}^{\infty} \mathrm{d}\dot{\delta}\ (\dot{\delta} - \dot{B})\, p(B, \dot{\delta})$, where $p(B, \dot{\delta})$ is the joint distribution of $\delta = B$ and $\dot{\delta} \equiv \mathrm{d}\delta/\mathrm{d}S$. Given that by the definitions eqs. (2.2) and (2.5) one has $\langle \delta^2 \rangle = S$ and $\langle \delta\dot{\delta} \rangle = 1/2$ (cf. also appendix A), the joint distribution $p(B, \dot{\delta})$ is a bivariate that can be written as the product of two Gaussians, one $p(B)$ with zero mean and variance S, and the other $p(\dot{\delta}|B)$ with mean $B\,\langle \delta\dot{\delta} \rangle / \langle \delta^2 \rangle = B/2S$ and variance $\langle \dot{\delta}^2 \rangle - \langle \delta\dot{\delta} \rangle^2 / \langle \delta^2 \rangle = (1 - \gamma^2)/4\gamma^2\, S$, in terms of the parameter $\gamma \equiv 1/\sqrt{4\, S\, \langle \dot{\delta}^2 \rangle}$.

Transforming from $\dot\delta$ to $\xi \equiv 2\gamma\sqrt{S}\,(\dot\delta - \dot B)$, the outcome writes

$$\begin{aligned}\nu\, f(\nu) &\simeq \frac{e^{-B^2/2\,S}}{\sqrt{2\pi}\,\gamma}\int_0^\infty \mathrm{d}\xi\;\xi\,\frac{e^{-(\xi-w)^2/2\,(1-\gamma^2)}}{\sqrt{2\pi\,(1-\gamma^2)}} = \\ &= \frac{w\,e^{-B^2/2\,S}}{\sqrt{2\pi}\,\gamma}\left\{\frac{1}{2}\,\mathrm{erfc}\left[-\frac{w}{\sqrt{2\,(1-\gamma^2)}}\right] + \sqrt{\frac{1-\gamma^2}{2\pi}}\,\frac{e^{-w^2/2\,(1-\gamma^2)}}{w}\right\}\,,\end{aligned} \tag{2.6}$$

in terms of the scaling variable ν of eq. (2.2) and of the quantity $w \equiv -2\,\gamma S\,\mathrm{d}[B(S)/\sqrt{S}]/\mathrm{d}S = \gamma\nu\,[1 + (1-2\,\eta)\,\beta\,\nu^{-2\,\eta}]$; for a constant ($\beta = 0$) or a square-root ($\eta = 1/2$) barrier, the latter just reads $w = \gamma\,\nu$. In these cases, the first crossing distribution can be put in the particularly simple form

$$\nu\, f(\nu) \simeq \frac{\nu\,e^{-(\nu+\beta)^2/2}}{\sqrt{2\pi}}\left\{\frac{1}{2}\,\mathrm{erfc}\left[-\frac{\Gamma\nu}{\sqrt{2}}\right] + \frac{e^{-\Gamma^2\,\nu^2/2}}{\sqrt{2\pi}\,\Gamma\nu}\right\}\,, \tag{2.7}$$

with $\Gamma \equiv \gamma/\sqrt{1-\gamma^2}$. As shown in appendix A the quantity Γ is a constant for a scale-invariant spectrum, but for a cold DM spectrum it instead depends on the scale ν (i.e., it depends on the scale S at given redshift, or equivalently on redshift at given scale S); this marks a break of self-similarity in the first crossing distribution, that actually appears to be indicated by some recent numerical simulations, and is at variance with what happens in the uncorrelated case. However, the dependence $\Gamma(\nu)$ is mild (see appendix A), hence to a first approximation it can be neglected and the value at $\nu \approx 1$ can be effectively adopted. Specifically, $\Gamma \approx 0.85$ and 0.51 apply for the Gaussian and the tophat filter, respectively.

In figure 2 we illustrate by the red lines how the upcrossing distribution of eq. (2.6) approximates very well the first crossing distribution derived by the Montecarlo method, both for a constant and a square-root barrier. We also plot, for comparison, other approximations that have been devised in the literature: the green line refers to the result for a constant barrier by [12], which is based on a perturbative path integral approach to the excursion set; the magenta lines illustrate the approximations by [32], which may be thought as the nonperturbative version of the path integral approach; the blue lines illustrate the result for complete correlation by [14], which considers deterministic walks with heights increasing monotonically as $\delta_R \propto \sqrt{S_R}$, and corresponds to the limit $\gamma \simeq 1$ in eq. (2.6); the cyan lines refer to the approximation by [33], which assumes the walk can be broken into independent segments with only internal correlations; the yellow lines illustrate for reference the result for a sharp $k-$space filter, corresponding to uncorrelated (Markovian) walks. In the bottom panel, the inset shows the residuals of these approximations with respect to the exact, Montecarlo outcome.

All in all, the approximation provided by the upcrossing distribution is by far the best compromise between simplicity and accurateness; e.g., for the square-root barrier the relative deviation amounts to $\Delta \log \nu\, f(\nu) \lesssim 0.1$ for $-1.5 \lesssim \log \nu^2 \lesssim 1$. We note, however, that when compared to the outcome from cosmological $N-$body simulations by [5], the first crossing distribution from excursion set theory, either exact or approximated, strongly underpredicts the number density of large mass objects (small S, large ν^2), and features a very different overall shape; actually it performs even worse than the uncorrelated case. A possible solution to such a shortcoming is discussed next.

2.2 Peaks as special positions

In the standard formulation of the excursion set theory, one assumes that halos may form equally likely at every point in space. However, $N-$body simulations suggest that the formation events occur preferentially around maxima, i.e. peaks, of the density field. The classic peaks theory tells us how to perform a weighted average of the walks over such special positions in the underlying field (see [14, 17–19, 22, 34]).

In peaks theory, the variable $x \equiv 2\gamma\sqrt{S}\,\dot{\delta} = \xi + 2\gamma\sqrt{S}\,\dot{B} \equiv \xi + \tau$ underlying eq. (2.6) basically represents the curvature of the density field (see [17], their section 5.2); this is strictly true only for Gaussian smoothing, but it holds to a good approximation also for tophat filtering. Thus an excursion set theory for peaks, or excursion set peaks, may be obtained just by accounting for the distribution of curvatures $F(x)$ around a peak position. Such a distribution is given by [18] (see their eq. A15)

$$F(x) = \frac{1}{2}\,(x^3 - 3\,x)\,\left[\mathrm{erf}\left(x\sqrt{\frac{5}{2}}\right) + \mathrm{erf}\left(x\sqrt{\frac{5}{8}}\right)\right] + \\ + \frac{2}{5\pi}\,\left[\left(\frac{31}{4}\,x^2 + \frac{8}{5}\right)\,e^{-5\,x^2/8} + \left(\frac{1}{2}\,x^2 - \frac{8}{5}\right)\,e^{-5\,x^2/2}\right]\,, \tag{2.8}$$

in terms of a function quite rapidly increasing with x; asymptotically, the expansions $F(x) \simeq 3^5\,5^{3/2}\,x^8/7 \times 2^{11}\,\sqrt{2\pi}$ for $x \ll 1$ and $F(x) \simeq x^3 - 3\,x$ for $x \gg 1$ apply.

Correspondingly, the first crossing distribution for the excursion set peak framework writes (see [23])

$$\nu\,f(\nu) \simeq \frac{e^{-B^2/2\,S}}{\sqrt{2\pi}\,\gamma}\,\frac{V}{V_\star}\,\int_0^\infty \mathrm{d}\xi\;\xi\,F(\xi+\tau)\,\frac{e^{-(\xi-w)^2/2\,(1-\gamma^2)}}{\sqrt{2\pi\,(1-\gamma^2)}}\,, \tag{2.9}$$

with $\tau \equiv 2\gamma\sqrt{S}\dot{B} = 2\,\eta\,\gamma\beta\,\nu^{1-2\,\eta}$; for a constant barrier $\tau = 0$, while for a square-root barrier $\tau = \gamma\beta$. In addition, $V/V_\star$ is a the ratio of the volume enclosed by the filter to a characteristic volume defined by [18]; such a ratio increases with ν, as detailed in appendix A.

Figure 3 illustrates that the net effect of including the peak constraints yields considerably more objects at the high-mass end relative to the upcrossing distribution, and an overall shape more similar to the $N-$body outcomes, especially for the square-root barrier. We will come back to the comparison of the excursion set peak results with numerical simulations at the end of Sect. 3.

3 Approximated excursion set peak

Now we aim at obtaining useful, approximated analytic expressions of the first crossing distribution for the excursion set peak framework. We start by deriving the asymptotic expansion of eq. (2.9) in the limit of small $S \ll \delta_c^2$ or $\nu \gg 1$, i.e., large masses and/or early times.

In this limit, $w \gg 1$ and the integral appearing in eq. (2.9) is dominated by large values of $\xi \simeq w$. Then we note that the integrand comprises two functions of ξ: a rapidly declining exponential, and the rapidly increasing function F; their product is a bell-shaped function with a clear maximum at a location $\bar{\xi}$, that suggests to try a Gaussian approximation. In other words we require in a neighborhood of $\xi \simeq \bar{\xi}$ that

$$F(\xi+\tau)\,e^{-(\xi-w)^2/2\,(1-\gamma^2)} \simeq F(\bar{\xi}+\tau)\,e^{-(\bar{\xi}-w)^2/2\,(1-\gamma^2) - \kappa\,(\xi-\bar{\xi})^2/2}\,, \tag{3.1}$$

with $\bar{\xi}$ and κ two quantities to be determined. At the zeroth order in ξ this expression is plainly true.

Requiring that it also holds at the first order implies

$$\frac{\mathrm{d}}{\mathrm{d}\xi}\left[F(\xi+\tau)\,e^{-(\xi-w)^2/2\,(1-\gamma^2)}\right]_{|\,\bar{\xi}}=0\ . \tag{3.2}$$

Since $\xi\simeq\bar{\xi}$ is supposed to be large, we can use the expansion $F(x)\simeq x^3-3\,x$; the result is the equation

$$3\,(1-\gamma^2)\,[(\bar{\xi}+\tau)^2-1]=(\bar{\xi}-w)\,(\bar{\xi}+\tau)\,[(\bar{\xi}+\tau)^2-3] \tag{3.3}$$

which yields the asymptotic expansion

$$\bar{\xi}\simeq w\left[1+\frac{3\,(1-\gamma^2)}{w^2}\right]\ . \tag{3.4}$$

Requiring that eq. (3.1) holds even at the second order implies

$$\frac{\mathrm{d}^2}{\mathrm{d}\xi^2}\left[F(\xi+\tau)\,e^{-(\xi-w)^2/2\,(1-\gamma^2)}\right]_{|\,\bar{\xi}}=-\kappa\,F(\bar{\xi}+\tau)\,e^{-(\bar{\xi}-w)^2/2\,(1-\gamma^2)}\ ; \tag{3.5}$$

the result is the equation

$$6\,(\bar{\xi}+\tau)-6\,[(\bar{\xi}+\tau)^2-1]\,\frac{\bar{\xi}-w}{1-\gamma^2}-\frac{[(\bar{\xi}+\tau)^2-3]\,(\bar{\xi}+\tau)}{1-\gamma^2}\left[1-\frac{(\bar{\xi}-w)^2}{1-\gamma^2}-\kappa\,(1-\gamma^2)\right]\ , \tag{3.6}$$

which after eq. (3.4) yields the asymptotic expansion

$$\kappa\simeq\frac{1}{1-\gamma^2}\left[1+\frac{3\,(1-\gamma^2)}{w^2}\right]\ . \tag{3.7}$$

Now we can substitute in eq. (2.9) the gaussian approximation eq. (3.1) to obtain

$$\nu\,f(\nu)\simeq\frac{e^{-B^2/2\,S}}{\sqrt{2\pi}\,\gamma}\,\frac{V}{V_\star}\,F(\bar{\xi}+\tau)\,\frac{e^{-(\bar{\xi}-w)^2/2\,(1-\gamma^2)}}{\sqrt{2\pi\,(1-\gamma^2)}}\int_0^\infty\mathrm{d}\xi\ \xi\,e^{-\kappa\,(\xi-\bar{\xi})^2/2}\ ; \tag{3.8}$$

the gaussian integral is trivial, while the function in front of it can be expanded with the help of eqs. (3.4) and (3.6) to yield

$$\begin{aligned}\nu\,f(\nu)\ \simeq\ &\frac{w\,e^{-B^2/2\,S}}{\sqrt{2\pi}\,\gamma}\,\frac{V}{V_\star}\ \left[w^3+3\,\tau\,w^2+3\,(1+\tau^2-2\,\gamma^2)\,w\right]\times\\ &\times\left\{\frac{1}{2}\,\mathrm{erfc}\left[-\frac{w}{\sqrt{2\,(1-\gamma^2)}}\right]+\sqrt{\frac{1-\gamma^2}{2\pi}}\,\frac{e^{-w^2/2\,(1-\gamma^2)}}{w}\right\}\ ;\end{aligned} \tag{3.9}$$

remarkably, this is the same result of the upcrossing distribution eq. (2.6), modulated by a function of w.

The approximation of eq. (3.9) strictly holds for large w, but can be improved so as to work pretty well in the whole range relevant for cosmological studies. To this purpose, note that when $w\ll 1$ then the integral in eq. (2.9) tends to a non-null constant; in our asymptotic expansion eq. (3.9) instead the modulating function in square brackets makes

everything to vanish in that limit. To recover the correct behavior for small w, it is sufficient to add in the square brackets a constant term; we find by trials that the value $(1+2\,\beta)\,(1-\gamma^2)$ works pretty well in yielding the exact result in the limit $w=0$ for diverse values of γ and β.

All in all, our approximation of the first crossing distribution for the excursion set peaks framework writes

$$\nu\,f(\nu) \simeq \frac{w\,e^{-B^2/2\,S}}{\sqrt{2\pi}\,\gamma}\,\frac{V}{V_\star}\,\mathcal{P}(w)\,\left\{\frac{1}{2}\,\mathrm{erfc}\left[-\frac{w}{\sqrt{2\,(1-\gamma^2)}}\right]+\sqrt{\frac{1-\gamma^2}{2\pi}}\,\frac{e^{-w^2/2\,(1-\gamma^2)}}{w}\right\}\,. \quad (3.10)$$

where we have defined the polynomial $\mathcal{P}(w) \equiv w^3+3\,\tau\,w^2+3\,(1+\tau^2-2\,\gamma^2)\,w+(1-\gamma^2)\,(1+2\,\beta)$.

For a constant or a square-root barrier with $w=\gamma\nu$ and $\tau=\gamma\beta$, the previous equation can be put in the remarkably simpler form

$$\nu\,f(\nu) \simeq \frac{\nu\,e^{-(\nu+\beta)^2/2}}{\sqrt{2\pi}}\,\frac{V}{V_\star}\,\mathcal{P}(\gamma\nu)\,\left\{\frac{1}{2}\,\mathrm{erfc}\left[-\frac{\Gamma\nu}{\sqrt{2}}\right]+\frac{e^{-\Gamma^2\,\nu^2/2}}{\sqrt{2\pi}\,\Gamma\nu}\right\}\,, \quad (3.11)$$

in terms of $\Gamma=\gamma/\sqrt{1-\gamma^2}$. The novel expressions in eqs. (3.10) and (3.11) constitute the main results of the present paper.

In figure 3 the comparison between the orange dotted and dashed lines (actually superimposed at the high-mass end) illustrates how efficiently the above expression approximate the exact result; e.g., for the square-root barrier the typical deviation amounts to $\Delta\log\nu\,f(\nu)\approx 0.05$ for $-1.5\lesssim\log\nu^2\lesssim 1.5$. It is seen that our approximation constitutes also a fair representation of the $N-$body outcome (see [5]; crosses); the inset shows the corresponding residuals. However, we notice that for a constant barrier the high-mass end is largely overpredicted, while for the square-root barrier it is slightly underpredicted. On the other hand, such a deficit of massive objects can be easily offset on considering the scatter in the value of the parameter β, as suggested by numerical simulations (see [1, 27, 28]). One can obtain the scattered first crossing distribution $\tilde{f}(S)$ just by convolving the distribution at fixed β from our approximations eqs. (3.10) and (3.11), with the distribution of β. For the sake of simplicity, we consider the outcome eq. (3.11) for a square-root barrier and a Gaussian scatter with mean value $\langle\beta\rangle=0.45$ and variance $\Sigma_\beta=0.35$, consistent with simulation indications. Since the dependence on β in the modulating function $\mathcal{P}(\gamma\nu,\gamma\beta)$ is mild, it can be neglected in performing the convolution. Then the result is analytic and reads

$$\begin{aligned}\nu\,\tilde{f}(\nu) &= \int \mathrm{d}\beta\,\frac{e^{-(\beta-\langle\beta\rangle)^2/2\Sigma_\beta^2}}{\sqrt{2\pi\Sigma_\beta^2}}\,\nu\,f(\nu) = \\ &= \frac{\nu\,e^{-(\nu+\beta)^2/2\,(1+\Sigma_\beta^2)}}{\sqrt{2\pi\,(1+\Sigma_\beta^2)}}\,\frac{V}{V_\star}\,\mathcal{P}(\gamma\nu)\,\left\{\frac{1}{2}\,\mathrm{erfc}\left[-\frac{\Gamma\nu}{\sqrt{2}}\right]+\frac{e^{-\Gamma^2\,\nu^2/2}}{\sqrt{2\pi}\,\Gamma\nu}\right\}\,;\end{aligned} \quad (3.12)$$

this expression constitutes a novel result. Note that for more complex barriers (e.g., $\eta>1/2$) or $\beta-$distributions (e.g., lognormal) the above convolution must be performed numerically, but the net effect is similar to what we have found.

The result, illustrated in figure 3 (bottom panel) by the orange solid line, reproduces very well the $N-$body outcome; it is seen from the residuals plotted in the inset that the relative deviation amounts to $\Delta\log\nu\,f(\nu)\lesssim 0.1$ for $-1.5\lesssim\log\nu^2\lesssim 1$. In terms of the characteristic

mass $M_\star(z)$ defined by $\delta_c^2(z) = S[M_\star(z)]$, the range translates into $M \gtrsim 10^{-2}\, M_\star$ at $z \approx 0$, $M \gtrsim 10^{-3}\, M_\star$ at $z \approx 1.5$, and practically encompasses all masses of cosmological interest for $z \gtrsim 1.5$.

Finally, in figure 4 we show that our approximation of Eq. (3.11) works excellently also for filters different from a tophat, and for power spectra different from a standard cold DM. To wit, we show the results for a Gaussian and tophat filters when scale-invariant power spectra are used in place of the standard cold DM one; a square-root barrier has been adopted for definiteness.

3.1 Halo bias

To show a direct application of our above results on halo abundance, we now focus now on deriving an approximated expression for the halo bias in the excursion set peak framework. The bias is the classical way of quantifying the connection between halo abundance and the environment (e.g., [35, 36]); recently, the topic has received a renewed interest in the context of correlated excursion set theory (see [37–40]).

The (Eulerian) halo bias is defined as

$$b = 1 + \frac{1}{\delta_{c0}} \left[\frac{N(M, \delta_c \to M_0, \delta_{c0})}{N(M, \delta_c)\, V} - 1 \right] \; ; \tag{3.13}$$

in the expression above what matters is the number of halos at redshift z with density contrast δ_c that will end up in an environment with volume V, mass $M_0 \simeq \bar{\rho} V \gg M$, and density contrast $\delta_{c0} \ll \delta_c$.

We will work under the peak-background split assumption, that corresponds to consider conditions where $\Delta S \simeq S \gg S_0$. Then the detailed computation of the conditional distribution appearing in eq. (3.13) is not really needed, since its shape is close to the unconditional distribution when written in terms of the appropriate scaling variable $\nu_c \equiv \Delta\delta_c/\sqrt{\Delta S}$. This is because the barrier of the conditional problem $B(S, \delta_c) - B(S_0, \delta_{c0}) \simeq B(S, \Delta\delta_c)$ tends to the unconditional one as $S \gg S_0$. On considering that $\nu_c \simeq \nu(1 - \delta_{c0}/\delta_c)$ and $f(\nu_c) \simeq f(\nu) - (\delta_{c0}/\delta_c)\, \nu f'(\nu)$ in the relevant limits $S \gg S_0$ and $\delta_c \gg \delta_{c0}$, one obtains

$$b(\nu) = 1 + \frac{1}{\delta_{c0}} \left[\frac{\nu_c\, f(\nu_c)}{\nu\, f(\nu)} - 1 \right] \simeq 1 - \frac{1}{\delta_c} \left[1 + \frac{\mathrm{d} \log f}{\mathrm{d} \log \nu} \right] \; . \tag{3.14}$$

Using for simplicity the expression eq. (3.12) for the square-root barrier with scatter we obtain

$$\begin{aligned} b(\nu) = 1 \; + \; & \frac{1}{\delta_c} \left\{ \frac{\nu^2 + \beta\nu}{1 + \Sigma_\beta^2} - 1 + \frac{1}{1 + \sqrt{\pi/2}\, \Gamma\nu\, e^{\Gamma^2\nu^2/2}\, \mathrm{erfc}[-\Gamma\nu/\sqrt{2}]} + \right. \\ & \left. - \; 3\, \frac{(\gamma\nu)^3 + 2\,\tau\,(\gamma\nu)^2 + (1 - 2\,\gamma^2 + \tau^2)\,\gamma\nu}{(\gamma\nu)^3 + 3\,\tau\,(\gamma\nu)^2 + 3\,(1 - 2\,\gamma^2 + \tau^2)\,\gamma\nu + (1 - \gamma^2)\,(1 + 2\,\beta)} - \left| \frac{\mathrm{d} \log V/V_\star}{\mathrm{d} \log \nu} \right| \right\} \; . \end{aligned} \tag{3.15}$$

Note that the last term is due to the $\nu-$dependence of the quantity $V/V_\star = (R/R_\star)^3$; it can be taken at an almost constant value ≈ 0.2 for the tophat filtering (cf. appendix A).

In figure 5 we show the results for uncorrelated excursion set (yellow line), for the upcrossing approximation to correlated excursion set (red line), and for our excursion set peak with scatter (orange line) from eq. (3.15). The latter reproduces fairly well the outcomes from

cosmological $N-$body simulations by [41] (crosses); as it can be seen from the residuals plotted in the inset, the relative deviation amounts to $\Delta \log \nu\, f(\nu) \approx 0.05$ for $-1.5 \lesssim \log \nu^2 \lesssim 1.5$. Such findings highlight that the peak constraint is a fundamental ingredient in understanding the halo bias.

4 Summary

The formation and evolution of DM halos constitutes a complex issue, whose attack ultimately requires cosmological $N-$body simulations on supercomputers.

However, some analytic modeling is most welcome to better interpret the simulation outcomes, to provide flexible analytic representations of the results, to develop strategies for future setups, and to quickly explore the effects of modifying the excursion set assumptions or the cosmological framework.

In this vein, we have derived approximated, yet very accurate, analytical expressions for the abundance and clustering of dark matter halos in the excursion set peak framework. The latter is based on the standard excursion set approach, but also includes the effects of a realistic filtering of the density field, of a mass-dependent threshold for collapse, and of the prescription from peak theory that halos tend to form around density maxima.

Our approximations works very well in reproducing the exact expressions for different power spectra, collapse barrier and density filters. When adopting a cold dark matter power spectra, a tophat filtering and a nonlinear (square-root) barrier with scatter, our approximated halo mass function and bias represent very well the outcomes of cosmological $N-$body simulations.

A Excursion set peak parameters

In this appendix we give some details on the computation of the parameters Γ, γ and $V/V_\star$ appearing in the main text.

The parameter Γ is defined as

$$\Gamma \equiv \frac{1}{\sqrt{4\, S\, \langle \dot\delta^2 \rangle - 1}}\ ; \tag{A.1}$$

and relatedly $\gamma \equiv \Gamma/\sqrt{\Gamma^2+1}$. To give an explicit expression for Γ, it is convenient to start from eqs. (2.1) and (2.5) that define the quantities $S = \langle \delta_R^2 \rangle$ and $C \equiv \langle \delta_R \delta_{R'} \rangle$ in terms of the power spectrum $P(k)$ and of the Fourier transform of the filter function $W_R(k)$. One has

$$\begin{aligned}
\partial_R S &= \frac{1}{2\pi^2} \int_0^\infty \mathrm{d}k\, k^2\, P(k) \partial_R W_R^2(k) \\
\partial_{R'} C_{|R'=R} &= \frac{1}{2\pi^2} \int_0^\infty \mathrm{d}k\, k^2\, P(k) W_R(k)\, \partial_R W_R(k) \\
\partial^2_{R,R'} C_{|R'=R} &= \frac{1}{2\pi^2} \int_0^\infty \mathrm{d}k\, k^2\, P(k) [\partial_R W_R(k)]^2
\end{aligned} \tag{A.2}$$

Combining these expressions yields $\langle \delta \dot\delta \rangle = \partial_{R'} C_{|R'=R} / \partial_R S = 1/2$, and $\langle \dot\delta^2 \rangle = \partial^2_{R,R'} C_{|R'=R} / (\partial_R S)^2$; finally, one finds

$$\Gamma = \left\{ \frac{\int_0^\infty \mathrm{d}k\ k^2\, P(k)\, W_R^2(k)\ \int_0^\infty \mathrm{d}k\ k^2\, P(k)\, [\partial_R W_R(k)]^2}{[\int_0^\infty \mathrm{d}k\ k^2\, P(k)\, W_R(k)\, \partial_R W_R(k)]^2} - 1 \right\}^{-1/2} . \tag{A.3}$$

The volume ratio $V/V_\star$ can be defined as $V/V_\star = (R/R_\star)^3$ in terms of the characteristic radius

$$R_\star \equiv \left(3\,\frac{R\,\partial_{R'} C_{|R'=R}}{\partial^2_{R,R'} C_{|R'=R}} \right)^{1/2} = \left[3\,\frac{\int_0^\infty \mathrm{d}k\; k^2\, P(k)\, W_R(k)\, R\,\partial_R W_R(k)}{\int_0^\infty \mathrm{d}k\; k^2\, P(k)\, [\partial_R W_R(k)]^2} \right]^{1/2} \quad . \tag{A.4}$$

Next we detail the computations for a cold DM, and for a scale-invariant power spectrum.

A.1 Scale-invariant power spectrum

When adopting a scale-invariant power spectrum $P(k) \propto k^n$, it is convenient to work in terms of the variable $x = kR$ since $W_R(k) = W(x)$ for both the Gaussian and tophat filters; then $\partial_R W_R(k) = k\,W'(x)$ holds, where the prime denotes derivative with respect to x.

For the Gaussian filter, one has

$$W_R(k) = e^{-x^2/2} \; . \tag{A.5}$$

Recalling the definition of the Euler Gamma function

$$\Gamma_{\rm E}(t) = 2\int_0^\infty \mathrm{d}x\; x^{2t-1}\, e^{-x^2} \tag{A.6}$$

and its basic property $\Gamma_{\rm E}(t+1) = t\,\Gamma_{\rm E}(t)$, from eqs. (A3) and (A4) it is easy to show that

$$\Gamma = \frac{\Gamma_{\rm E}\left(\frac{n+5}{2}\right)}{\Gamma_{\rm E}\left(\frac{n+7}{2}\right)\,\Gamma_{\rm E}\left(\frac{n+3}{2}\right) - \Gamma_{\rm E}\left(\frac{n+5}{2}\right)} = \sqrt{\frac{n+3}{2}} \; . \tag{A.7}$$

and that

$$\frac{V}{V_\star} = \left[\frac{\Gamma_{\rm E}\left(\frac{n+7}{2}\right)}{3\,\Gamma_{\rm E}\left(\frac{n+5}{2}\right)} \right]^{3/2} = \left(\frac{n+5}{6} \right)^{3/2} \quad . \tag{A.8}$$

For the tophat filter, one has

$$W_R(k) = \frac{3}{x}\, j_1(x) \qquad\qquad W'(x) = \frac{3}{x}\,\left[j_0(x) - \frac{3}{x}\, j_1(x) \right] \tag{A.9}$$

with $j_0(x) \equiv \sin x/x$ and $j_1(x) = (\sin x - x\cos x)/x^2$ the spherical Bessel functions of the first kind. It is convenient to define the three integrals

$$I_{00} \equiv \int_0^\infty \mathrm{d}x\; x^{n+2}\, j_0^2(x) \qquad I_{01} \equiv \int_0^\infty \mathrm{d}x\; x^{n+1}\, j_0(x)\, j_1(x) \qquad I_{11} \equiv \int_0^\infty \mathrm{d}x\; x^n\, j_1^2(x) \tag{A.10}$$

and using the properties of the Bessel functions to compute the ratios

$$\frac{I_{00}}{I_{11}} = \frac{n\,(n-1)\,(n-3)}{4\,(n+1)} \qquad\qquad \frac{I_{01}}{I_{11}} = \frac{3-n}{2} \; . \tag{A.11}$$

Exploiting eqs. (A3) and (A4) yields, after some tedious algebra,

$$\Gamma = \frac{|3\,I_{11} - I_{01}|}{\sqrt{I_{11}\,I_{00} - I_{01}^2}} = \sqrt{\frac{(n+1)\,(n+3)}{n-3}} \; , \tag{A.12}$$

and

$$\frac{V}{V_\star} = \left(3\,\frac{|3\,I_{11} - I_{01}|}{I_{00} + 9\,I_{11} - 6\,I_{01}} \right)^{3/2} = \left[\frac{n\,(n+5)}{6\,(n+1)} \right]^{3/2} \quad . \tag{A.13}$$

Note that to ensure convergence of the integrals in eqs. (A10) and positivity of Γ^2 and $(V/V_\star)^2$ it is required that the spectral index falls in the range $-3 < n < -1$.

A.2 Cold DM power spectrum

For the cold DM power spectrum, both Γ (or $\gamma = \Gamma/\sqrt{1+\Gamma^2}$) and $V/V_\star$ depend on scale. In figure 6 we plot these quantities as a function of the scaling variable ν for both the Gaussian and tophat filters.

As to Γ, the dependence on ν^2 can be represented to better than 5% in the range $-1.5 \lesssim \log\nu^2 \lesssim 1.5$ by the following expression:

$$\log\Gamma \simeq \Gamma_0 + \Gamma_1 \, \log\nu^2 + \Gamma_2 \, (\log\nu^2)^2 \; ; \tag{A.14}$$

the fitting parameters $(\Gamma_0, \Gamma_1, \Gamma_2)$ amount to $(-0.071, 0.119, -0.019)$ for the Gaussian and $(-0.291, 0.086, -0.030)$ for the tophat filtering. The dependence on ν is mild (almost logarithmic), and can be neglected to a first approximation in the excursion set expressions; taking the values $\Gamma \approx 0.85$ (or $\gamma \approx 0.65$) and 0.51 (or $\gamma \approx 0.46$) corresponding to $\nu \approx 1$ for the Gaussian and tophat filtering works pretty well.

As to $V/V_\star$, the following expression applies:

$$\log V/V_\star \simeq V_0 + V_1 \, \log\nu^2 + V_2 \, (\log\nu^2)^2 \; , \tag{A.15}$$

with parameters (V_0, V_1, V_2) amounting to $(-0.459, 0.121, 0.009)$ for the Gaussian and to $(-0.179, 0.172, 0.036)$ for the tophat filtering.

Acknowledgments

Work supported in part by INAF and MIUR. We thank the anonymous referee for helpful and constructive comments. We acknowledge stimulating discussions with A. Cavaliere, P.S. Corasaniti, and P. Salucci. A.L. is grateful to SISSA for warm hospitality.

References

[1] R.K. Sheth, H.J. Mo, and G. Tormen, *Ellipsoidal collapse and an improved model for the number and spatial distribution of dark matter haloes*, *MNRAS* **323** (2001) 1

[2] V. Springel, et al., *Simulations of the formation, evolution and clustering of galaxies and quasars*, *Nature* **435** (2005) 629

[3] M.S. Warren, K. Abazajian, D.E. Holz, and L. Teodoro, *Precision Determination of the Mass Function of Dark Matter Halos*, *ApJ* **646** (2006) 881

[4] D.S. Reed, R. Bower, C.S. Frenk, A. Jenkins, and T. Theuns, *The Halo Mass Function into the Dark Ages*, *MNRAS* **374** (2007) 2

[5] J. L. Tinker, et al., *Toward a Halo Mass Function for Precision Cosmology: The Limits of Universality*, *ApJ* **688** (2008) 709

[6] S.G. Murray, C. Power, and A.S.G. Robotham, *How well do we know the halo mass function?*, *MNRAS* **434** (2013) L61

[7] W.A. Watson, I.T. Iliev, A. D'Aloisio, A. Knebe, P.R. Shapiro, and G. Yepes, *The halo mass function through the cosmic ages*, *MNRAS* **433** (2013) 1230

[8] J.R. Bond, S. Cole, G. Efstathiou, and N. Kaiser, *Excursion set mass functions for hierarchical gaussian fluctuations*, *ApJ* **379** (1991) 440

[9] P.S. Corasaniti, and I. Achitouv, *Toward a Universal Formulation of the Halo Mass Function*, *Phys Rev. L.* **106** (2011) 1302

[10] R.I. Epstein, *Proto-galactic perturbations*, *MNRAS* **205** (1983) 207

[11] A. Lapi, P. Salucci, and L. Danese, *Statistics of dark matter halos from the excursion set approach*, *ApJ* **772** (2013) 85

[12] M. Maggiore, and A. Riotto, *The halo mass function from excursion set theory. I. Gaussian fluctuations with non-markovian dependence on the smoothing scale*, *ApJ* **711** (2010) 907

[13] M. Musso, and R.K. Sheth, *One step beyond: the excursion set approach with correlated steps*, *MNRAS* **423** (2012) L102

[14] A. Paranjape, T.-Y. Lam, and R.K. Sheth, *Halo abundances and counts-in-cells: the excursion set approach with correlated steps*, *MNRAS* **420** (2012) 1429

[15] W.H. Press, and P. Schechter, *Formation of Galaxies and Clusters of Galaxies by Self-Similar Gravitational Condensation*, *ApJ* **187** (1974) 425

[16] R.K. Sheth, and G. Tormen, *An excursion set model of hierarchical clustering: ellipsoidal collapse and the moving barrier*, *MNRAS* **329** (2002) 61

[17] L. Appel, and B.J.T. Jones, *The Mass Function in Biased Galaxy Formation Scenarios*, *MNRAS* **245** (1990) 522

[18] J.M. Bardeen, J.R. Bond, N. Kaiser, and A.S. Szalay, *The statistics of peaks of Gaussian random fields*, *ApJ* **304** (1986) 15

[19] J. Bond, and S. Myers, *The Peak-Patch Picture of Cosmic Catalogs. I. Algorithms*, *ApJS* **103** (1996) 1

[20] A. Manrique, A. Raig, J.M. Solanes, G. Gonzalez-Casado, P. Stein, and E. Salvador-Sole, *The Effects of the Peak-Peak Correlation on the Peak Model of Hierarchical Clustering*, *ApJ* **499** (1998) 548

[21] K. Jedamzik, *The cloud-in-cloud problem in the press-schechter formalism of hierarchical structure formation*, *ApJ* **448** (1995) 1

[22] M. Nagashima, *A Solution to the Missing Link in the Press-Schechter Formalism*, *ApJ*, **562** (2001) 7

[23] A. Paranjape, R.K. Sheth, and V. Desjacques, *Excursion set peaks: a self-consistent model of dark halo abundances and clustering*, *MNRAS* **431** (2013) 1503

[24] *Planck* Collaboration 2013, *Planck 2013 results. XVI. Cosmological parameters*, *A&A*, in press [preprint arXiv:1303.5076]

[25] N. Sugiyama,*Cosmic Background Anisotropies in Cold Dark Matter Cosmology* , *ApJS* **100** (1995) 281

[26] V.R. Eke, S. Cole, and C.S. Frenk, *Cluster evolution as a diagnostic for Omega*, *MNRAS* **282** 263

[27] B.E. Robertson, A.V. Kravtsov, J. Tinker, and A.R. Zentner, *Collapse barriers and halo abundance: testing the excursion set ansatz*, *ApJ* **696** (2009) 636

[28] G. Despali, G. Tormen, and R.K. Sheth, *Ellipsoidal halo finders and implications for models of triaxial halo formation*, *MNRAS* **431** (2013) 1143

[29] A.J. Benson, et al., *Dark matter halo merger histories beyond cold dark matter - I. Methods and application to warm dark matter*, *MNRAS* **428** (2013) 1774

[30] A.R. Zentner, *The Excursion Set Theory of Halo Mass Functions, Halo Clustering, and Halo Growth*, *Journ. Mod. Phys.* **16** (2007) 763

[31] J. Zhang, and L. Hui, *On random walks with a general moving barrier*, *ApJ* **641** (2006) 641

[32] A. Farahi, and A. Benson, *Excursion set theory for correlated random walks*, *MNRAS* **433** (2013) 3428

[33] J.A. Peacock, and A.F. Heavens, *Alternatives to the Press and Schechter cosmological mass function*, *MNRAS* **243** (1990) 133

[34] A. Paranjape, and R.K. Sheth, *Peaks theory and the excursion set approach*, *MNRAS* **426** (2013) 2789

[35] H.J. Mo, and S.D.M. White, *An analytic model for the spatial clustering of dark matter haloes*, *MNRAS* **282** (1996) 347

[36] R.K. Sheth, and G. Tormen, *Large-scale bias and the peak background split*, *MNRAS* **308** (1999) 119

[37] A. Faltenbacher, and S.D.M. White, *Assembly bias and the dynamical structure of dark matter halos*, *ApJ* **708** (2010) 469

[38] C.-P. Ma, M. Maggiore, A. Riotto, and J. Zhang, *The bias and mass function of dark matter haloes in non-Markovian extension of the excursion set theory*, *MNRAS* **411** (2011) 2644

[39] A. Paranjape, E. Sefusatti, K. C. Chan, V. Desjacques, P. Monaco, R.K. Sheth, *Bias deconstructed: unravelling the scale dependence of halo bias using real-space measurements*, *MNRAS* **436** (2013) 449

[40] J. Zhang, C.-P. Ma, and A. Riotto, *Dark-matter halo assembly bias: environmental dependence in the non-markovian excursion-set theory*, *ApJ* **782** (2014) 44

[41] J.L. Tinker, et al., *The large-scale bias of dark matter halos: numerical calibration and model tests*, *ApJ* **724** (2010) 878

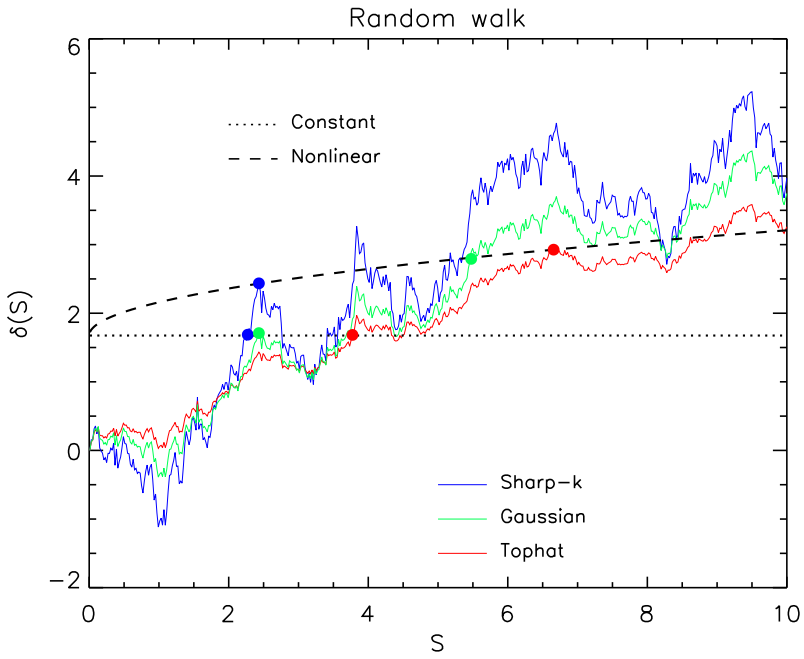

Figure 1. Examples of random walks executed by the overdensity contrast δ_R as a function of the variance S_R, when a sharp k-space (blue line), a Gaussian (green line) or a tophat (red line) smoothing filter is adopted. The dotted and dashed lines illustrate the constant and square-root barrier at redshifts $z = 0$; the dots illustrate the location of first crossing. It is easily seen that the random walks for the gaussian and tophat filters vary less erratically than that for the sharp $k-$space, as a consequence of the correlations between the steps.

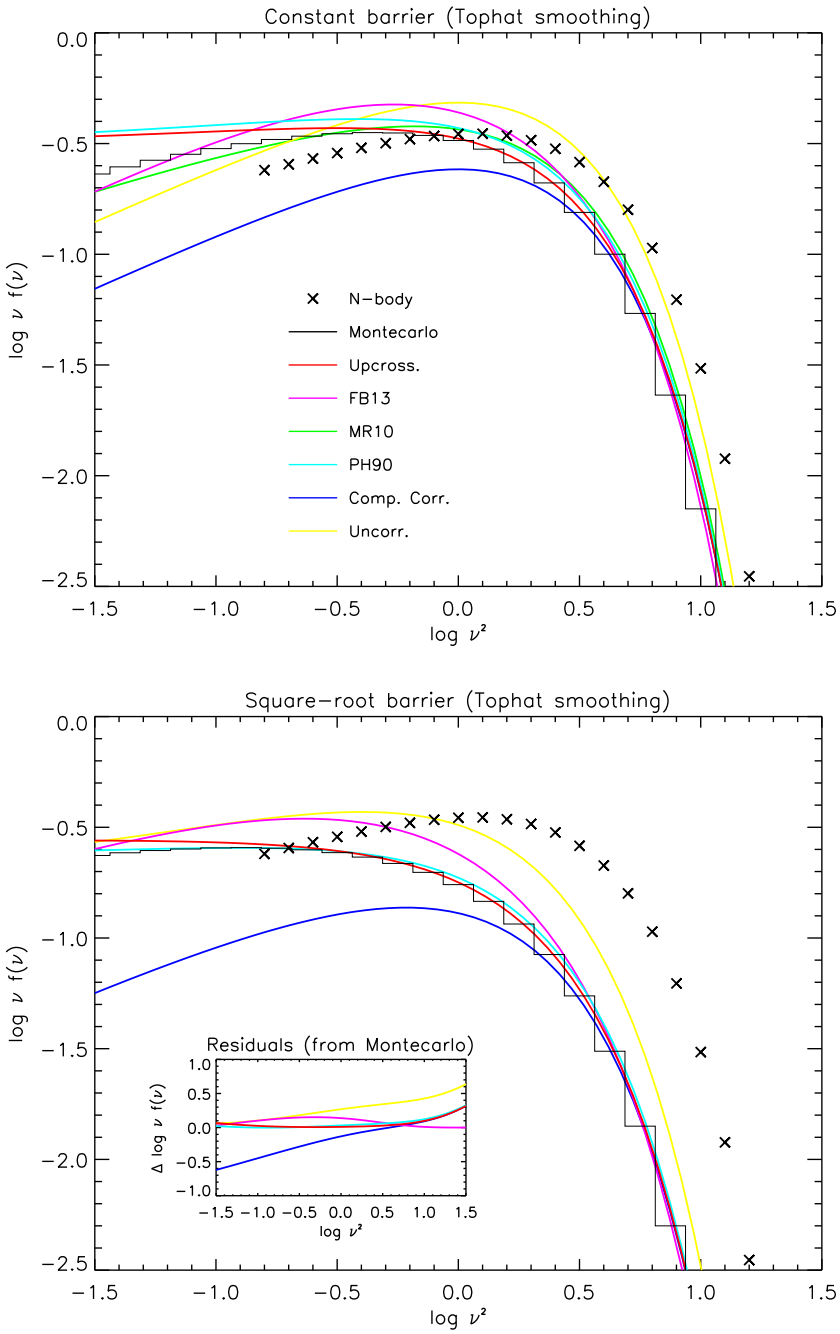

Figure 2. First crossing distribution for a tophat smoothing filter, adopting a constant (top panel) or a square-root (bottom panel) barrier after eq. (2.2) and the standard excursion set theory prescription. The black histogram refers to the exact solution from Montecarlo simulations, red line to the upcrossing approximation by [8, 13], magenta line to the approximation by [32], green line to the approximation by [12], cyan line to the approximation by [33], blue line the completely correlated limit by [14], and yellow line to the result for a sharp $k-$space. Crosses illustrate the outcomes of cosmological $N-$body simulations from [5]. In the bottom panel, the inset shows the residuals with respect to the Montecarlo outcome.

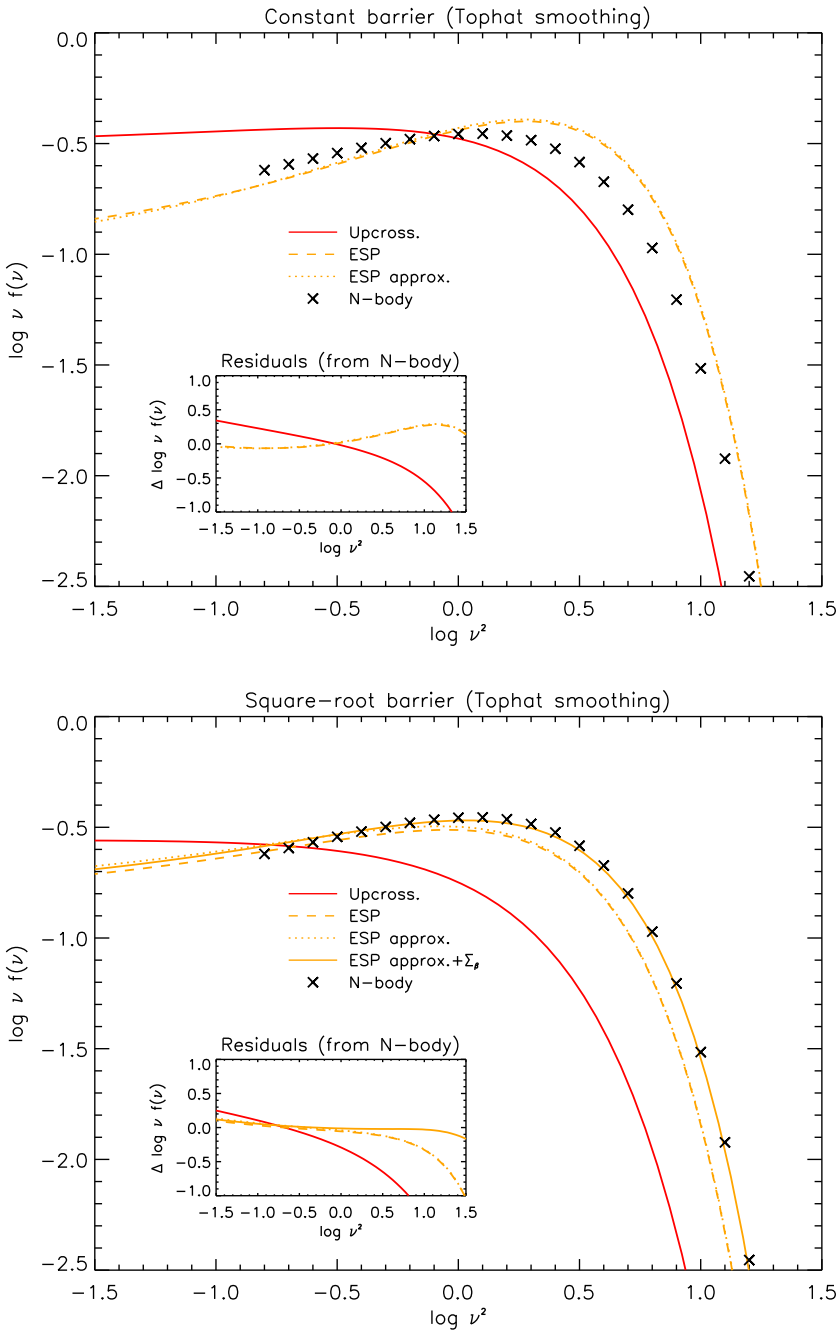

Figure 3. First crossing distribution for a tophat smoothing filter, adopting a constant (top panel) or a square-root (bottom panel) barrier and the excursion set peak prescription. Red line is the result for the standard excursion set approach (actually the upcrossing approximation, as in figure 2), dashed orange line refers to the exact result for the excursion set peak (cf. eq. 2.9), dotted line is our approximation of eqs. (3.10) and (3.11), and solid line in the bottom panel includes the scatter on the barrier after eq. (3.12). Crosses illustrate the outcomes of cosmological $N-$body simulations from [5]. In both panels the inset shows the residuals with respect to the $N-$body outcome.

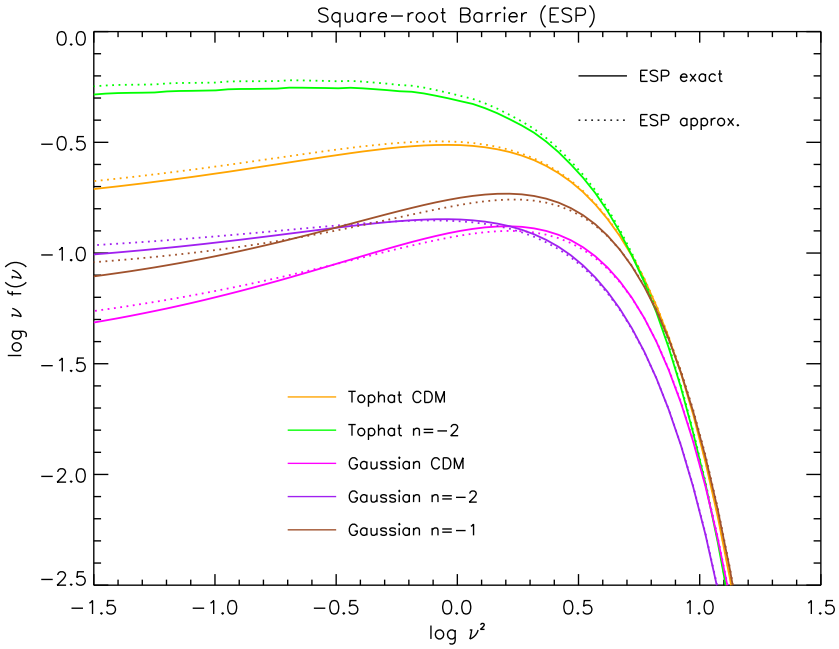

Figure 4. First crossing distribution for a tophat smoothing filter, adopting a square-root barrier after eq. (2.2) and the excursion set peak prescriptions. Solid lines illustrate the exact result after eq. (2.9), and dashed line is our approximation of eq. (3.11). As detailed in the legend, orange and green lines refer to a tophat smoothing filter and the standard cold DM or a scale invariant power-spectrum with index $n = -2$; magenta, purple and brown lines refer to a Gaussian smoothing filter and a cold DM or scale-invariant power spectrum with index $n = -2$ and $n = -1$.

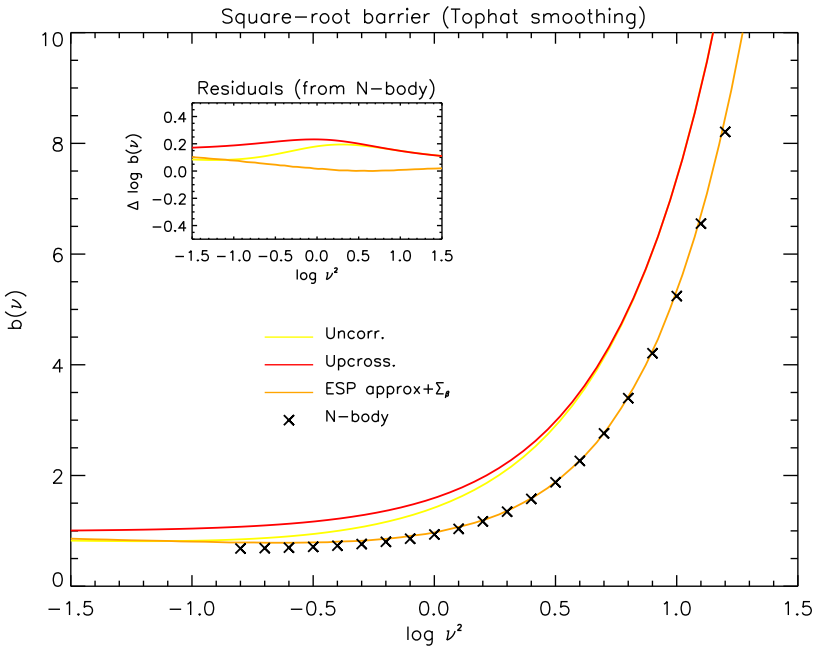

Figure 5. Halo bias in the background-split approximation, for a tophat smoothing filter and a square-root barrier. Yellow line refers to uncorrelated (Markovian) walks, red line to the upcrossing approximation for correlated excursion set theory, and orange line to our approximation for the excursion set peak of eqs. (3.14) and (3.15). Crosses illustrate the outcomes of cosmological $N-$body simulations from [41]. The inset shows the residuals with respect to the $N-$body outcome.

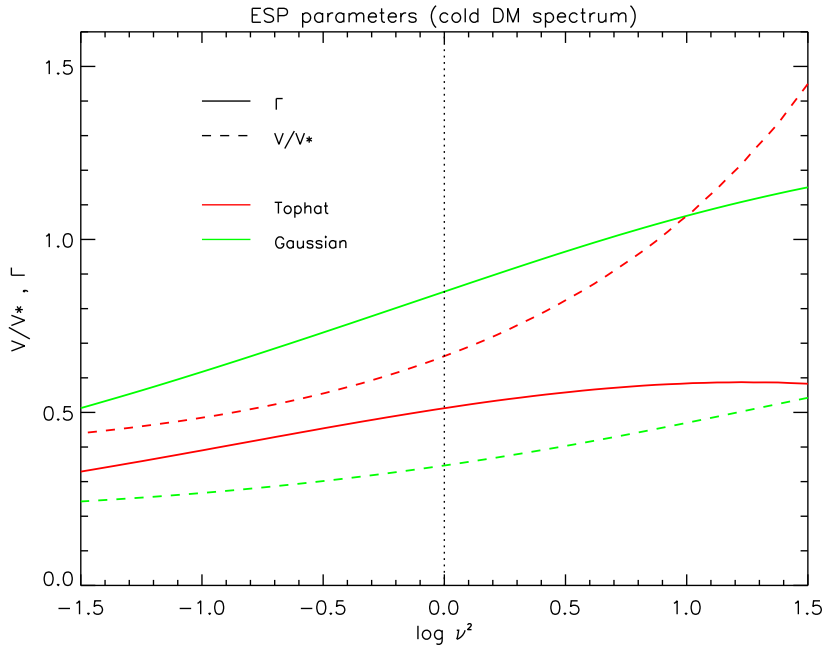

Figure 6. Excursion set peak parameters Γ (solid lines) and $V/V_\star$ (dashed lines) as a function of the scaling variable ν, for Gaussian (green) and tophat (red) filtering, cf. appendix A. The vertical dotted line marks the location $\nu = 1$.